



CHORUS

This is the accepted manuscript made available via CHORUS. The article has been published as:

Valence nucleon populations in the Ni isotopes

J. P. Schiffer, C. R. Hoffman, B. P. Kay, J. A. Clark, C. M. Deibel, S. J. Freeman, M. Honma, A. M. Howard, A. J. Mitchell, T. Otsuka, P. D. Parker, D. K. Sharp, and J. S. Thomas

Phys. Rev. C **87**, 034306 — Published 6 March 2013

DOI: [10.1103/PhysRevC.87.034306](https://doi.org/10.1103/PhysRevC.87.034306)

Valence nucleon populations in the Ni isotopes

J. P. Schiffer,^{1,*} C. R. Hoffman,¹ B. P. Kay,^{1,†} J. A. Clark,¹ C. M. Deibel,^{1,2,‡} S. J. Freeman,³ M. Honma,⁴
A. M. Howard,^{3,§} A. J. Mitchell,^{3,¶} T. Otsuka,⁵ P. D. Parker,⁶ D. K. Sharp,³ and J. S. Thomas³

¹*Physics Division, Argonne National Laboratory, Argonne, Illinois 60439, USA*

²*Joint Institute for Nuclear Astrophysics, Michigan State University, East Lansing, Michigan 48824, USA*

³*School of Physics and Astronomy, University of Manchester, Manchester M13 9PL, United Kingdom*

⁴*Center for Mathematical Science, University of Aizu, Aizu-Wakamatsu, Fukushima 965-8580, Japan*

⁵*Department of Physics and Center for Nuclear Study, University of Tokyo, Hongo,
Tokyo 113-0033, Japan and RIKEN, Hirosawa, Wako-shi, Saitama 351-0198, Japan*

⁶*A. W. Wright Nuclear Structure Laboratory, Yale University, New Haven, Connecticut 06520, USA*

(Dated: February 19, 2013)

Measurements of neutron-adding, neutron-removing and proton-adding reactions were carried out for the four stable even Ni isotopes. Particular attention was paid to obtaining precise values of the cross sections at the peaks of the angular distributions. Tests with sum rules for the neutron data indicate that the results are self consistent at the level of a few tenths of a nucleon. Data on proton-adding reactions were also obtained, and analyzed with a slightly different method—while these data are also consistent, the ambiguities are larger. The occupancies of the neutron orbits derived from the data, the proton vacancies and the energy centroids of the neutron, neutron-hole, and proton single-particle excitations are obtained. The data also provide some estimate about the closure of the $0f_{7/2}$ shell. The results are compared to shell-model calculations, and may serve as a reference point for future exploration.

The understanding of nuclear structure in terms of the shell model has been remarkably successful in describing many of the observed features of nuclei. Nucleon transfer reactions have been essential in relating these models to experimentally measurable quantities, and specifically single-particle overlaps. The energies of single-particle states based on most stable nuclei have been mapped out by measurements of nucleon-adding and nucleon-removing transfer reactions. The present paper gives a test case of the consistency of the procedures used in extracting such information from transfer reactions, using measurements based on the stable Ni isotopes and elaborates on a short summary that has been published in [1].

The doubly-magic nucleus ^{56}Ni is expected to be reasonably described as the closure of the $0f_{7/2}$ shell with 28 neutrons and 28 protons. Just beyond ^{56}Ni , in the four stable Ni isotopes with an even number of neutrons, the neutron orbits $1p_{3/2}$, $0f_{5/2}$, and $1p_{1/2}$ are not separated by much in energy and thus are filling more-or-less at the same rate. The subshell of 40 nucleons is not very strongly defined, and the $0g_{9/2}$ state, at slightly higher energy, may or may not participate appreciably in the filling process in the stable isotopes. The proton orbits above $Z = 28$ are, at least nominally, vacant.

Populations of the valence nucleons may be mapped

out by measurements of the nucleon-adding and -removing transfer reactions, utilizing the Macfarlane and French [2] sum rules. These sum rules express how the summed reduced cross sections for transitions with a given value of j^π are related to the number of vacancies or particles in that orbit. For neutron transfer on the Ni isotopes, there are numerous earlier experiments, for example [3–5], which have been summarized and evaluated in [6]. These measurements had established the rate of filling approximately, but measurements of the various reactions and isotopes were carried out at different times, sometimes at different energies and with different instruments and analyzed with slightly different assumptions and parameters. Thus, the quantitative accuracy of the results has not been tested in a consistent procedure. In an earlier Letter [1] we discussed the internal consistency in the neutron transfer reactions, the procedure of summing the neutron-adding and neutron-removing strengths, utilizing the sum rules to give consistent normalizations and the additional consistency in the filling of the neutron orbits. No assumptions about the filling of the $0f_{7/2}$ sub-shell had to be made. In the present paper, we discuss the procedure for neutrons in somewhat more detail and point out some of the limitations of the method used. We include the measurements of proton-transfer reactions which have also been studied previously, for instance by [7, 8], and are evaluated in [6]. Our results are summarized and compared with shell-model calculations.

I. EXPERIMENTAL METHOD

Precision accelerators with the requisite energies and suitable magnetic spectrographs are on the verge of ex-

* E-mail: schiffer@anl.gov

† Present address: Physics Department, University of York, Heslington, York YO1 5DD, United Kingdom

‡ Present address: Department of Physics and Astronomy, Louisiana State University, Baton Rouge, Louisiana 70803, USA

§ Present address: Department of Physics, University of Notre Dame, Notre Dame, Indiana 46556, USA

¶ Present address: Department of Physics, University of Massachusetts Lowell, Lowell, Massachusetts 01854, USA

inction. The present measurements were carried out to obtain an accurate set of cross sections under consistent conditions. The intent was to test the extent to which transfer reactions can yield quantitative information in a procedure that minimizes the ambiguities in extracting spectroscopic overlaps while satisfying the sum rules, and attempt to minimize reliance on a particular formalism or set of model parameters.

The experiment was carried out at the recently closed Yale ESTU tandem accelerator and split-pole spectrograph with its focal plane detector system. The method was one that has been used before [9] to measure both neutron-adding and -removing reactions at similar energies, after the target thicknesses were calibrated by α -particle scattering at a far sub-Coulomb energy ($E_\alpha = 9$ MeV) in the regime of Rutherford scattering. The transfer yields were measured using the *same* spectrograph aperture, target, beam collimation, and beam integrator as in the calibration runs, to minimize systematic errors. The bombarding energies for deuterons and protons were chosen to be sufficiently above the Coulomb barriers to give the distinctive patterns, well understood in reaction theory, yet low enough to get optimal energy resolution in the spectrograph and to cover roughly similar ranges of energies in the incident and outgoing channels.

The reactions, energies and angles used, along with the energy resolution achieved are summarized in Table I and typical calculated angular distributions are shown in Fig. 1. The angular width of the aperture was ± 20 mrad horizontally and ± 40 mrad vertically, with the central setting accurate to about 1 mrad. The angles at which the measurements were made for (d,p) and (p,d) reactions were slightly different because of the calculated shift arising from differences in kinematics. The smaller variation from the range of Q values was generally less than the experimental errors and assumed to be correctly accounted for in the distorted wave Born approximation (DWBA) calculations.

We did not attempt to measure angular distributions in this work. There have been extensive studies on transfer reactions on the Ni isotopes and the ℓ -value assignments are consistent. Our focus was to obtain a consistent set of peak cross sections, measured with good accuracy. In the previous studies the observed peaks in the cross sections were in good agreement with those calculated with DWBA. The variation in the calculated peak positions with different distorting parameters is on the order of 0.2° , and the sensitivity of the peak cross section to angle is less than 1% for a variation of 1° . The peak angles in the calculated angular distributions over the range of targets and Q values is less than about 1° . The sensitivity both to the accuracy in the measurement of angle to the calculated variations in peak angles over the range of these measurements, and to the distorting parameters used in the DWBA is such that the choice of peak angle for the measurement is not a significant source of uncertainty.

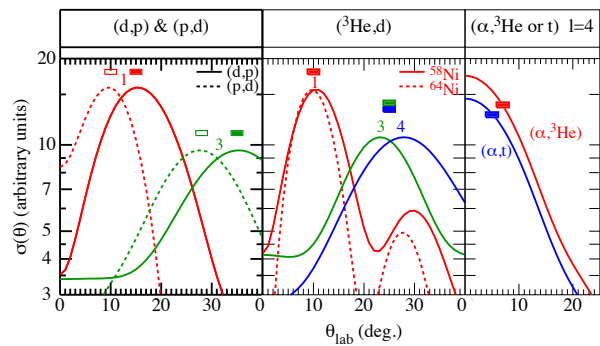


FIG. 1. (Color online) Calculated DWBA angular distributions for the (d,p) reaction on ^{60}Ni at $E_d = 10$ MeV (full lines) and for the (p,d) reaction at $E_p = 28$ MeV (dashed lines), for a full or empty orbit respectively. The $\ell = 1$ calculations are for $j = 3/2$, the $\ell = 3$ for $5/2$, and the $\ell = 4$ for $9/2$. The full and empty bars represent the angles at which measurements were made, with the width of the bars indicating the angular aperture of the spectrograph. The proton transfer is shown in the middle box, and the α -induced reactions on the right.

The $(\alpha,^3\text{He})$ and $(^3\text{He},\alpha)$ reactions were measured to gain more reliable information for the higher ℓ transitions, since in these reactions the momentum difference between incident and outgoing channels favors higher values of ℓ . The momentum matching and its influence on cross sections is illustrated in Fig. 2. The Born approximation is expected to be more reliable at the peaks of the angular distributions, where the cross sections are relatively large. For the reactions involving α particles, the angular distributions peak at 0° and decrease by only a few percent at the angles at which the measurements were carried out; the data were analyzed assuming that the reaction theory correctly accounted for this.

For proton transfer, only the adding reactions $(^3\text{He},d)$ and (α,t) were measured, since $Z = 28$ is nominally a closed shell. The discussion regarding neutron transfer applies to these reactions as well. The angles for the measurements were chosen to be at or near maxima in the calculated angular distributions. These are also given in Table I and examples are shown in Fig. 1.

The targets were self-supporting films of isotopically enriched Ni, $160\text{-}219 \mu\text{g}/\text{cm}^2$ thick. Precise values of the target thicknesses were deduced from Rutherford scattering at 9 MeV and 20° in the laboratory and are given in Table II, along with known isotopic purities. The absolute uncertainties in these target thicknesses are estimated to be $\sim 7\%$, dominated by the uncertainty in the aperture size, with the remaining uncertainties in the angle, current integrator, beam location on the target, and statistics each on the order of a percent. However, most of these uncertainties cancel in the ratios between the sub-Coulomb calibration and the transfer data. The beams were less than 2 mm in diameter and care was taken that the same portion of the target be irradiated in the Rutherford-scattering measurements and the var-

TABLE I. Energies, angles and measured resolutions for each reaction type.

Reaction	Beam energy (MeV)	θ_{LAB} (deg)	FWHM (keV)
(d, p)	10	15	33
		35	
(p, d)	28	10	48
		25	
$(\alpha, {}^3\text{He})$	38	7	50
$({}^3\text{He}, \alpha)$	25	5	75
$({}^3\text{He}, d)$	18	10	50
		25	
(α, t)	38	5	64

ious subsequent reactions.

TABLE II. The measured target thicknesses and their isotopic purities.

Nucleus	Thickness ($\mu\text{g}/\text{cm}^2$)	Purity (%)
${}^{58}\text{Ni}$	211	99.6
${}^{60}\text{Ni}$	204	99.7
${}^{62}\text{Ni}$	219	96.5
${}^{64}\text{Ni}$	160	91.0

The measurements were carried out over a five-day period with the split-pole spectrograph and focal-plane detector system. The detector was a position-sensitive ionization drift chamber filled with 150 Torr of isobutane, which gives position and energy-loss information and was backed by a scintillator that gives the total energy of the light ions [10]. Outgoing particles were identified through a series of 2-D spectra related to energies and positions measured in the focal plane as shown in Figs. 3 and 4. Multiple gates provided unambiguous identification and it is estimated that the gating does not contribute to the cross section uncertainties in a significant way. Focal-plane position spectra were energy calibrated using the known energies of strongly populated states [6]. Average resolutions achieved with the various targets and reactions are given in Table I and typical spectra are shown in Fig. 5.

Yields were determined from fits to the data using a Gaussian distribution to approximate the line shape in the spectra. For states that were closely spaced a simultaneous fit to several Gaussians was done, constraining the widths to be equal. Several independent fits to the data indicate a systematic uncertainty of less than a percent for cross sections greater than a mb, and a few percent for cross sections below this. Isotopic impurities in the target, in particular in ${}^{64}\text{Ni}$ (with $\sim 5\%$ ${}^{58}\text{Ni}$ and $\sim 3\%$ ${}^{60}\text{Ni}$) did not interfere with the extraction of yields from nearby states. Contaminants such as isotopes

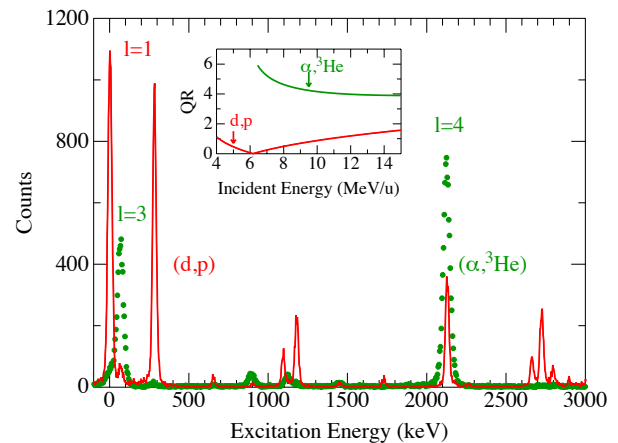


FIG. 2. (Color online) Spectra for the ${}^{60}\text{Ni}(d,p)$ and $(\alpha, {}^3\text{He})$ reactions at 15° and 7° , respectively, indicating the strong enhancement of the lower ℓ values in the former reaction and the higher ones in the latter. The inset shows the reason for this: the momentum matching for the two reactions as a function of bombarding energy, (deduced from a crude semi-classical picture), where the arrows show the bombarding energies used in this work, and Q is the momentum transfer and R the radius.

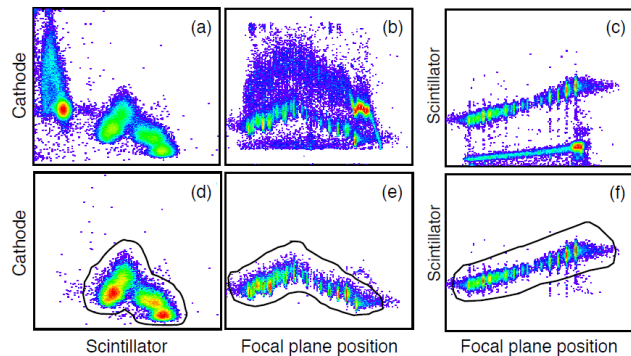


FIG. 3. (Color online) Cuts on the focal plane detector to identify particles from the ${}^{58}\text{Ni}(d,p)$ reaction at 15° . In the upper row, (a) shows the ungated cathode vs. scintillator pulse height, (b) the cathode vs. focal-plane position, and (c) the scintillator pulse height vs. position. The lower row in (d), (e), and (f) shows the same quantities gated. The black lines indicate the gates—thus (f) shows the cathode vs. focal-plane position gated on the black regions shown in (d) and (e). Note that the irregular behavior of the cathode signal in the middle panels results from a non-uniformity in the grid wire spacing; this did not affect the focal-plane position spectrum and could be readily handled by drawing appropriate particle identification gates in these 2-d spectra.

of oxygen and carbon were typically not found in the excitation energy region of interest. In select cases where they did appear [e.g. ${}^{64}\text{Ni}(d,p)$], the contaminant peaks did not interfere with the ${}^{65}\text{Ni}$ states of interest.

The cross sections were obtained from the measured

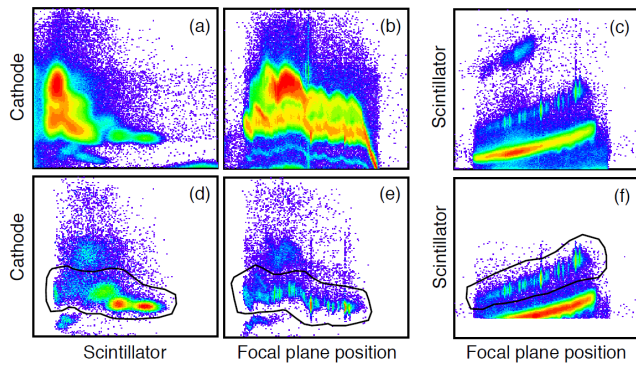


FIG. 4. (Color online) Same as Fig. 3 for the $^{58}\text{Ni}(\alpha, ^3\text{He})$ reaction at 7° .

yields (Y) from

$$\sigma = \frac{Y}{n_b} \cdot F_R, \quad (1)$$

where n_b is the number of beam particles measured over the counting period, and F_R is a scale factor determined for each target by the low-energy, sub-Coulomb α scattering. The values of Y and n_b from the calibration measurements yield values of F_R for each target,

$$F_R = \frac{n_b}{Y \cdot \epsilon} \cdot \sigma_R(20^\circ), \quad (2)$$

with ϵ representing the purity of the target (see Table II), and $\sigma_R(20^\circ)$ the Rutherford cross section in mb/sr. Apparent in Equations 1 and 2, is that the relatively large systematic uncertainty in the absolute size of the aperture ($\sim 7\%$) becomes irrelevant when the same setting is used consistently. The same is true of the absolute target thickness, with the assumption that the deposited layer is sufficiently uniform on the scale of 1-2 mm, and that the changes in the location of the beam spot are no greater than this.

The remaining systematic uncertainties sum to a few percent for the absolute cross sections and may be due to target thickness variations, movement of the incoming beam, and the change in Rutherford cross sections from small uncertainties in the measuring angle. Including statistics, uncertainties in the absolute cross sections are estimated as 4% for $\sim \sigma > 1$ mb/sr, $\sim 7\%$ for $0.1 < \sigma < 1.0$ mb/sr, and $\sim 18\%$ for $\sigma < 0.1$ mb/sr.

The states that are significantly populated in transfer reactions on the Ni isotopes are known from previous work [6] and their spins determined. The emphasis in the present measurement is to obtain a set of accurate cross section data that may be analyzed in a consistent manner. The question of contributions from possible missed states was discussed in [1] and likely is negligibly small.

Some confirmation of the previously determined spins is shown in Fig. 6. Here, the ratio of the cross sections between the reactions involving deuterons and alphas is plotted against the ratio of the deuteron cross sections at

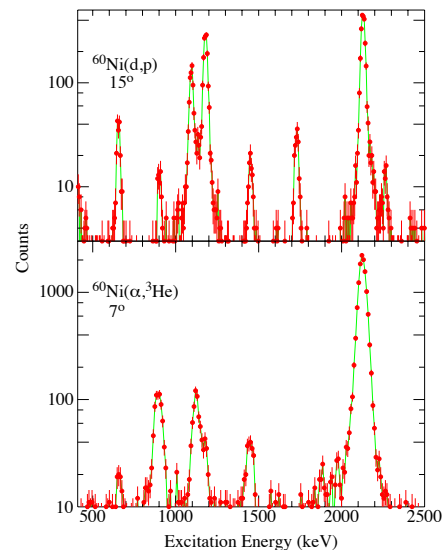


FIG. 5. (Color online) To illustrate the experimental resolution and the level of background in the final gated spectra, the same part of the excitation energy in ^{61}Ni is shown from the neutron-adding reactions. The spectra are normalized such that the height of each peak is the cross section leading to the corresponding state.

the two angles. These ratios are sensitive to the difference between $\ell = 1$ and 3, and not sensitive to that between $\ell = 3$ and 4. However, as may be seen from the figure, all the significant cross sections appear to be consistent with the previously assigned ℓ values.

II. SPECTROSCOPIC FACTORS AND DWBA

The question of whether spectroscopic factors are ‘true observables’ was discussed in our brief report of this work [1]. There is no question that spectroscopic factors are model dependent, at least in some measure. However, the sum rules based on spectroscopic factors can be a valuable, even if approximate, tool for learning about nuclei and nuclear properties. Since spectroscopic factors are essentially reduced cross sections, we use the reaction theory, in the present case DWBA, only as a crutch to help handle what may be regarded as kinematic aspects of the reaction, such as the different energies, Q values, effects of distorting parameters in the entrance and exit channel, and the form factors. Other reaction models might serve equally well. We measure, as well as we can, the cross sections for all the states populated in adding and removing a nucleon from a given target. The same reaction is used for adding as removing e.g. (d, p) and (p, d) or $(\alpha, ^3\text{He})$ and $(^3\text{He}, \alpha)$. The summed reduced cross sections then provide a natural normalization of what might be considered the ‘single-particle strength’ in a reasonably consistent description [1]. In this section we give some of the details of the procedure and the re-

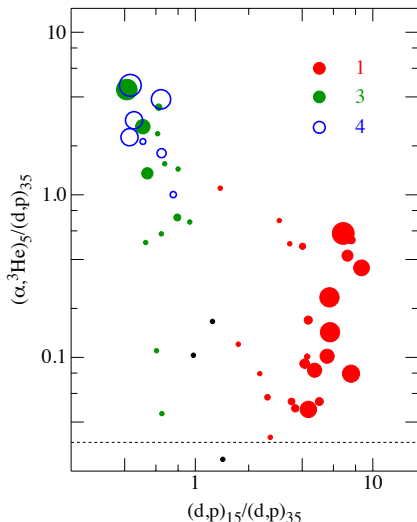


FIG. 6. (Color online) Ratios of the measured cross sections for neutron-adding reactions, with the subscripts on the axis labels indicating the angle of measurement. Different colors are used to represent the expected ℓ values, and the area of the points reflects the relative cross sections within each group. The open (blue) symbols are $\ell = 4$ transitions, the filled ones are $\ell = 1$ (red) or 3 (green). The angular-momentum transfer for all the data shown is known from other experiments, and the consistency with the previous assignments, particularly for the strongest and most important transitions, is demonstrated for $\ell = 1$ transitions compared to the higher ℓ transfers. The black dots represent weak transitions whose angular momenta are unknown or doubtful.

sults. This procedure was used for neutron transfer only. For protons, we relied on the assumption that $Z = 28$ was a good closed shell, an assumption that was found to be approximate.

A. Neutron transfer

Calculations of cross sections within the framework of DWBA were carried out with the Ptolemy [11] code using the Reid bound-state wave function for deuterons, in the case of (d, p) and (p, d) reactions, and Woods Saxon potentials to approximate the internal wave functions of ^3He , ^3H , and ^4He .

For neutron transfer, to obtain an accurate measure of the occupancies, the spectroscopic factors need to be normalized and the procedure for this has been described [1]. We obtained the normalization N by

$$N \equiv \frac{1}{(2j+1)} [\Sigma(2j+1)C^2 S_{\text{adding}} + \Sigma C^2 S_{\text{removing}}] \quad (3)$$

This was done both for deuteron ($\ell = 1$) and alpha-induced ($\ell = 3$ and 4) reactions, and the normalizations were quite similar as is shown in Table III for one set of distorting parameters. The uncertainties in these normalizations are more a matter of possible missed states

and/or problems with the reaction formalism—and, although these factors are not believed to be large, they are difficult to estimate. The experimental cross sections are estimated to be accurate to better than 4%. The variations in the four independent determinations are shown in the table as a measure of the validity of the procedure and of possible uncertainties. These seem to be around ~ 5 , 7, and 8% for the $\ell = 1$ and $\ell = 3$ (d, p) , and $(\alpha, ^3\text{He})$ transitions respectively, suggesting that the additional uncertainties in the analysis may be comparable to the uncertainties in cross sections.

TABLE III. Normalization factors for neutron transfer.

Nucleus	$N_{\ell=1}$	$N_{\ell=3}$	$N_{\ell=3,\alpha}$
^{58}Ni	0.527	0.528	0.518
^{60}Ni	0.548	0.503	0.464
^{62}Ni	0.558	0.554	0.471
^{64}Ni	0.566	0.480	0.433
Mean	0.550(15)	0.517(28)	0.471(30)

In effect, since the experiment determined both neutron-adding and neutron-removing cross sections under similar kinematic conditions and the DWBA analysis was carried out with consistent ‘global’ optical-model parameters, the extracted spectroscopic factors depend only weakly on reaction theory. The global parameters used were those of Ref. [12] for the deuterons and those of Ref. [13] for protons, allowing for the variation of parameters with target nucleus, and with energy. Other global parameters for protons [14] gave spectroscopic factors that were only slightly different from these. This is illustrated in Fig. 7. The ratios of peak cross sections from the DWBA calculations with the two sets of proton parameters were 1.03 ± 0.04 , and there is a slight dependence that would alter the balance between occupancies and vacancies for the two parameter sets by $\sim 5\%$.

The values of the normalization $N_{\ell=1}$ are listed in Table IV for the combined $\ell = 1$ ($1/2^-$ and $3/2^-$) strengths, since some of the spin assignments are ambiguous. The normalizations given are for different potential parameters, some fixed in energy and nucleus, some global parameters, variable with energy, A , and $N - Z$. Different bound-state parameters make a rather large difference in the absolute value of the normalization. The values marked ‘fixed’ in Table IV allowed for no variation in the parameters, other than the $A^{1/3}$ dependence of potential radii. The bound-state parameters used were generally those of Ref. [15] ($1.28A^{1/3}$) that were chosen to give reasonable fits to the charge distributions. In some cases bound-state parameters with smaller radii that were consistent with those of the global optical-model parameters in the low-energy neutron limit [14], as well as [13], $\sim 1.17A^{1/3}$ were used. The rms fluctuation in the normalization among the isotopes is expressed in the \pm values. The parameter set adopted for the spectroscopic factors used in Ref. [1] are those on the 4th line of Ta-

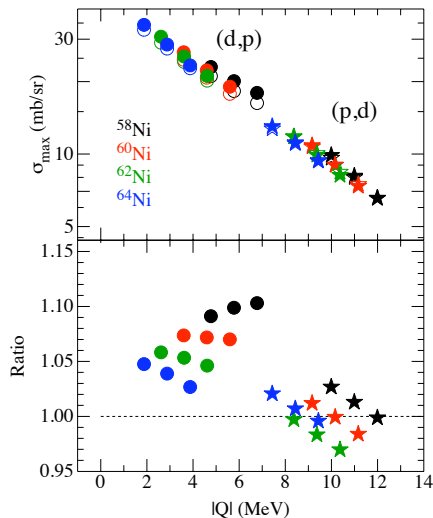


FIG. 7. (Color online) On the top, the DWBA calculated peak cross sections are plotted for $\ell = 1$ transitions with two proton potentials from [13] (solid) and [14] (open), for both (d,p) and (p,d) reactions, for Q values corresponding to the first 2 MeV of excitation energy in the final nucleus. On the bottom, the ratios of the cross sections for the two potentials are shown.

ble IV, the deuteron potentials of Ref. [12], the proton potentials of Ref. [13], and the bound-state parameters of Ref. [15].

Other parameters for the distorting parameters were also used, some with no variation with energy or target. While the absolute values of the normalization factors obtained (for the average of the four targets) using the above procedures differed for different parameter sets, the normalized spectroscopic factors varied by much less. The largest variations in spectroscopic factors arose from the bound-state form factor ($\sim 30\%$), while for a fixed form factor the variation was less ($\sim 8\%$).

TABLE IV. Normalization factors for $\ell = 1$ neutron transfer.

Deuteron	Proton	Bound State	Normalization
[12], fixed	[13], fixed	[15]	0.492 ± 0.020
[16]	[13], fixed	[15]	0.646 ± 0.041
[17]	[13]	[15]	0.568 ± 0.037
[12]	[13]	[15]	0.550 ± 0.015
[18]	[19]	[15]	0.572 ± 0.051
[12]	[13]	[13]	0.475 ± 0.018
[12]	[14]	[14]	0.561 ± 0.022

Since the ratio of normalizations for $\ell = 1$ and 3 cross sections depends somewhat on the choice of radii for the bound states, the normalization for the two ℓ values should be considered separately. The j values also matter. To illustrate this dependence on bound-state parameters, we show the ratios for different j values of DWBA cross sections with changes in the bound-state

geometry in Fig. 8. The wavefunction of the transferred neutron is always calculated with the depth of the potential adjusted to yield the specified binding energy. As is shown in the figure, both the radial wave functions for different ℓ values and the $j = \ell \pm 1/2$ nature of the orbits matter. For reasonable parameter choices the differences can be on the order of $\sim 5\%$. The uncertainty is worse, perhaps $\sim 20\%$, for the $g_{9/2}$ spectroscopic factors, since no independent normalization was possible for this transition and it had to rely on that for the $f_{5/2}$ transitions. However, in the germanium isotopes, a similar test was performed, and there the $9/2^+$ strength was observed cleanly for both the adding and removing reactions [9]. With the bound-state parameters of Ref. [15] the normalizations for $\ell = 3$ and 4 by the above procedure were the same to within $\sim 3\%$, giving some empirical justification for using the $f_{5/2}$ normalization for both. It is worth noting that the majority of the earlier analyses (e.g. in the 1960's) of transfer data in terms of DWBA were carried out before systematic analyses of scattering with polarized proton beams were available and thus before it was appreciated that the radius of the spin-orbit term should be considerably smaller than the radius of the real potential [20]. Using the larger radius for the spin-orbit term meant a substantially greater dependence of $(2j+1)C^2S$ on j than the more recent values of r_{so} that are 20-30% smaller than r_0 .

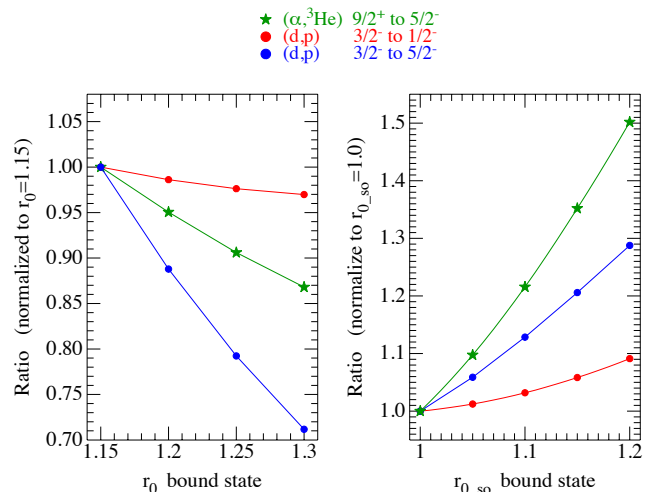


FIG. 8. (Color online) The sensitivity of ratios of calculated DWBA cross sections to choice of radial parameters for the potential used to calculate the wave function of the transferred neutron. Plotted are the ratios of states with different ℓ and j . On the left the variation with the radius of the central potential is explored, and the different slopes indicate that the dependence on ℓ is dominant. On the right the radius of the spin-orbit part of the potential is varied.

The spectroscopic factors measured for $\ell = 3$ transitions by various pairs of reactions: (d,p) and $(\alpha, ^3\text{He})$, (p,d) and $(^3\text{He},\alpha)$, $(^3\text{He},d)$ and (α,t) reactions are compared in Fig. 9. For strong transitions the agreement is excellent, but for weaker ones the ratios of spectro-

scopic factors fluctuate considerably. It is important to point out that the sums are dominated by the strong transitions, and thus even a factor of two discrepancy in a transition with a spectroscopic factor that is two orders of magnitude smaller than that for the strongest ones (~ 0.02 mb/sr in the $({}^3\text{He},\alpha)$ reactions instead of ~ 2 mb/sr), represents only a $\sim 1\%$ variation in the sum. The momentum matching for (d,p) , (p,d) and $({}^3\text{He},d)$ is rather poor for $\ell = 3$ compared to the reactions involving α particles – a miss-match in momentum transfer means that the direct one-step cross sections are smaller and more complicated multi-step reactions may become dominant at a level of S that is an order of magnitude greater than for a well-matched transition. That is why we adopted the spectroscopic factors from the better-matched reactions – and the deviations are more a reflection of the problems with poorly-matched reactions. The data suggest that multi-step processes could be significant for transitions with cross sections less than a few hundred $\mu\text{b/sr}$. Nevertheless, these discrepancies between pairs of reactions can be used to set an order-of-magnitude estimate on how meaningful spectroscopic factors are for weak reactions, as will be discussed below. Since for weak transitions, the order of magnitude of the deviations in S derived from the poorly-matched and well-matched reactions are about 0.03, and about an order of magnitude in cross section is lost in the poorly matched reactions, we estimate a constant uncertainty in S in the well-matched reaction at the level of perhaps 0.003 in S for adding (and in $S/(2j+1)$ for removing) reactions.

It is interesting to note that the values of the various normalization constants that were obtained from the summing procedure, ~ 0.5 - 0.6 , are close to the values of ‘absolute’ spectroscopic factors obtained from $(e,e'p)$ measurements on closed-shell nuclei [21] from ${}^{16}\text{O}$ to ${}^{208}\text{Pb}$. This quenching of spectroscopic factors was explained in terms of short-range correlations [22]. The consistency among the four targets also confirms the implicit assumption, that any modifications in spectroscopic factors from correlations is a uniform property of the nuclear medium. It is not changing from nucleus to nucleus, or between particle and hole excitations. Calculations of spectroscopic factors from models of nuclear structure do not include such correlations and the values obtained in the present work, by requiring that the sum rule be satisfied, are the appropriate ones to compare to those calculated from the shell model.

The values of neutron spectroscopic factors are listed in the Appendix A. The cross sections have been deposited with the Nuclear Data Center [23].

1. Estimate of uncertainties in spectroscopic factors.

The uncertainties in cross sections were discussed above and estimated as $\sim 4\%$ for the strongest transitions and as much as 18% for cross sections below 0.1 mb/sr.

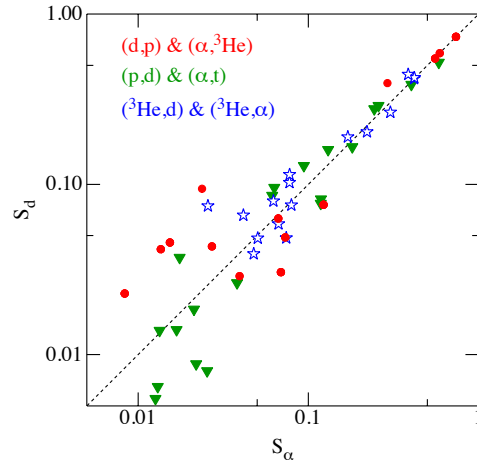


FIG. 9. (Color online) The ratio of spectroscopic factors for $\ell = 3$ transitions obtained from the cross sections for pairs of reactions, including proton transfer. The S_d axis is for the (d,p) (p,d) and $(d,{}^3\text{He})$ reactions, the S_α axis for the $(\alpha,{}^3\text{He})$, $({}^3\text{He},\alpha)$, and (α,t) ones. For the nucleon-removal reactions $S/(2j+1)$ is plotted. The figure illustrates some of the uncertainties in deriving spectroscopic factors for weaker transitions: the consistency for the strongest transitions and increasing divergence for weaker ones.

The uncertainties in spectroscopic factors are more complicated and difficult to estimate, because they also depend on the assumptions of the reaction theory and on the choice of parameters. Much of the paper is concerned with discussions of these factors. Most sensitive, within DWBA, is the choice of parameters for the bound state, as was seen in Fig. 8, though this can be reduced to the extent that the bound-state radial parameters may be constrained. Perhaps a more serious problem is in the applicability of DWBA for weak transitions, where in Fig. 9 one sees that values are consistent between two reactions for strong transitions but not for weak ones. From such data one may perhaps argue that in addition to the uncertainties in cross sections there is a *constant* limiting uncertainty, perhaps on the order of ± 0.005 in S for adding and in $S/(2j+1)$ for removing for well-matched reactions, and several times that for reactions that are mismatched by 2 or more units in ℓ . This then is likely the dominant uncertainty for the weakest transitions, where large contributions from higher-order mechanisms may contribute to the cross section. But it has no significant effect on the occupancies and vacancies derived from the sum rules. These multistep amplitudes are coherent with the direct ones, a further reason for the qualitative nature of these estimates.

Attempting to combine these factors and noting that they are strongly dependent on assumptions, a rough estimate of the uncertainties in spectroscopic factors for the well-matched reactions are as follows. For strong

transitions that are greater than ~ 0.2 the uncertainty is about 10%, in comparison to spectroscopic factors derived with different assumptions and $\sim 6\%$ relative uncertainty compared to strong spectroscopic factors obtained with the same assumptions. Similarly, for transitions whose strengths are between 0.03 and 0.2 of the full value, we estimate an uncertainty of $\sim 15\%$, and for transitions below 0.03, 25%, with an additional *constant* uncertainty of perhaps 0.005 in S for adding (and $S/(2j+1)$ for removing).

2. Incompleteness of the $f_{7/2}$ shells.

We started out with the assumption that ^{56}Ni represents a good doubly closed shell. Our data can provide a test of the validity of this assumption in the sum of the spectroscopic factors for nucleon addition to states with $j^\pi = 7/2^-$. If the $f_{7/2}$ shell were perfectly closed and the reaction mechanism simple one-nucleon addition, these sums should be zero. The sums are finite, though small, and thus have relatively larger fractional uncertainties because of possible second-order, two-step mechanisms that may contribute to weak transitions as was demonstrated in Fig. 9 above.

The observed $7/2^-$ sums are shown in Fig. 10, including measurements for neutrons and protons, which are discussed later. It seems that these ‘prohibited’ sums tend to get larger the closer the nucleus is to $N(Z) = 28$, suggesting that the shell becomes increasingly complete a few nucleons away from the closed shell. The uncertainties shown in the figure attempt to reflect a crude estimate of possible contributions from second-order processes in the reaction. If one were to assume these sums at face value, it implies that in ^{58}Ni , for instance, there is on the order of 12%, or ~ 0.5 neutrons, missing from the closed shell. These vacancies would then have to be filled as part of the occupancy of the $1p$ and $0f_{5/2}$ orbitals. The normalization procedure that was followed for neutrons would *not* be affected by this deficiency in shell closure, because the sums of occupancies and vacancies were used.

The missing $f_{7/2}$ strength should however show up in the neutron occupancies of the shells beyond that, the sum of the $1p$, $0f_{5/2}$, and $0g_{9/2}$ occupancies. These were plotted in Fig. 3 of Ref. [1], where 2.0, 4.1, 5.9 and 8.3 were seen for $^{58,60,62,64}\text{Ni}$ respectively, with 2.0, 4.0, 6.0, and 8.0 expected for a perfect $N, Z = 28$ shell. Adding in the $f_{7/2}$ holes would change these *expected* total occupancies to 2.5, 4.2, 6.2, and 8.1, in slightly worse agreement (~ 0.3 nucleon rms deviation rather than ~ 0.2) but still within the estimated uncertainties.

3. Centroids

The energy centroids (mean excitation energies for a given j weighted by spectroscopic factors) were com-

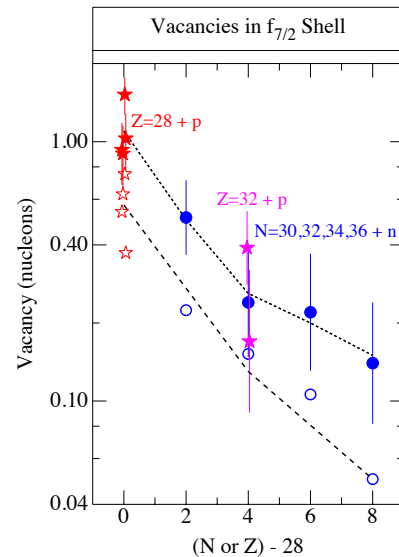


FIG. 10. (Color online) The apparent vacancies in the $f_{7/2}$ shell deduced from neutron and proton-adding reactions are shown as a function of the number of nucleons outside the 28 shell as full symbols. The four points shown as red stars are from proton adding and are a measure of the completeness of the $f_{7/2}$ proton shell, while the full blue circular dots indicate the apparent vacancies for neutrons in the four Ni isotopes. The purple stars are from an earlier measurement on proton adding to the germanium isotopes [24]. The heavy black short-dashed line is to highlight the trend in the experimental data as a function of distance from the closed shell. The error bars shown are rough qualitative estimates, based mostly on the estimated uncertainties from competing higher-order reaction mechanisms. The empty circles and stars represent the corresponding quantities from shell-model calculations with the GXPF1A interaction.

puted for the neutron transfer reactions and are shown in Fig. 11. The values of the energy centroids are listed in Table V. The large uncertainty for the $3/2^-$ and $1/2^-$ neutron-addition centroids at $A = 62$ are due to ambiguities regarding the spins of several $\ell = 1$ states, and therefore these uncertainties are anti-correlated; an overall uncertainty of 75 keV is estimated as a rough approximation to allow for possible weak, missed states at high excitation energy.

B. Proton transfer

For ^3He and α -particles optical potentials have not been studied as extensively for their dependence on energy, A or $N - Z$ as for nucleons and deuterons, but because the interaction is dominated by absorption, these features are less critical. The potentials used were from [25] and [26].

The normalization procedure was different from that used for neutrons, relying on the *assumption* that $Z = 28$ is a closed shell. The normalization for protons is there-

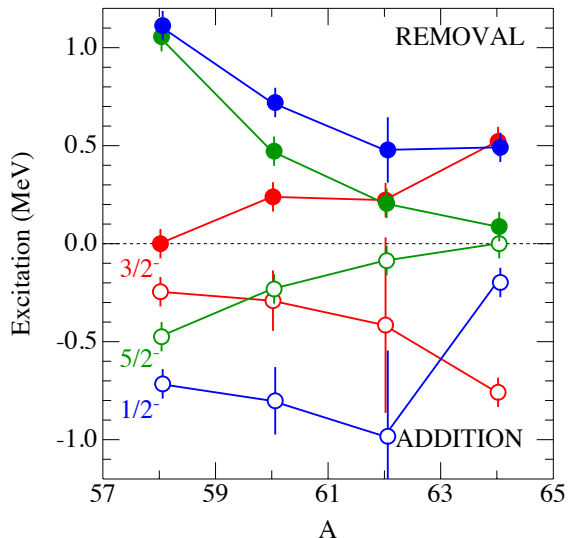


FIG. 11. (Color online) The centroid of the experimental, spectroscopic-factor-weighted excitation energies are plotted for neutron-addition (vacancies, open circles) and neutron-removal (occupancies, full circles). The error bars reflect estimated uncertainties, including those from uncertain spin assignments.

fore subject to greater uncertainty, as is discussed below. For proton adding, two isospin states are possible with the upper isospin states occurring at too high an excitation energy to have been accessible in this experiment. Instead, the relevant correction was made using the neutron-adding spectroscopic factors, since the proton-adding $T_>$ states are the isobaric analogs of the neutron-adding states and have the same spectroscopic factors [27]. Since all the relevant proton orbits are assumed to be unoccupied, for a given orbit j on a spin-zero target

$$\text{Vacancies} = \sum (2j+1) \frac{2T}{2T+1} S_{<} + \sum (2j+1) \frac{1}{2T+1} S_{>} \quad (4)$$

where the squares of the Clebsch-Gordan coefficients C^2 are written out explicitly, and $S_{<}$ and $S_{>}$ are the spectroscopic factors for $T_{<}$ and $T_{>}$ states. The spectroscopic factors for $T_{>}$ are taken from the (d, p) or $(\alpha, {}^3\text{He})$ reactions discussed above. This upper isospin component is most important for ${}^{58}\text{Ni}$.

It may be noted that, in general, the upper isospin component also has to be included for neutron removal on targets with a neutron excess. However, for the valence neutrons of the Ni isotopes there is no significant occupancy in the corresponding proton orbits, and therefore in the consideration of neutron orbits in the above discussion the relevant proton-removal spectroscopic fac-

TABLE V. Centroid Energies for Single-Neutron (Hole) Strength (keV).

Reaction	J^π	A	Expt.	GXPFI1A	JUN45
Adding	$3/2^-$	58	245(75)	483	224
		60	291(150)	619	339
		62	416(450)	790	766
		64	758(75)	843	964
$\text{rms}_{\text{expt.} - \text{theor.}}$				275	245
Adding	$5/2^-$	58	475(75)	826	659
		60	231(75)	436	164
		62	87(75)	401	85
		64	0(75)	191	145
$\text{rms}_{\text{expt.} - \text{theor.}}$				274	122
Adding	$1/2^-$	58	715(75)	1034	1599
		60	801(170)	447	930
		62	983(440)	500	485
		64	198(75)	150	172
$\text{rms}_{\text{expt.} - \text{theor.}}$				340	511
Removing	$3/2^-$	58	0(75)	238	0
		60	239(75)	265	196
		62	222(75)	537	248
		64	521(75)	1161	581
$\text{rms}_{\text{expt.} - \text{theor.}}$				376	39
Removing	$5/2^-$	58	1056(75)	888	1119
		60	472(75)	499	649
		62	205(75)	201	154
		64	87(75)	439	124
$\text{rms}_{\text{expt.} - \text{theor.}}$				195	99
Removing	$1/2^-$	58	1113(90)	1322	1989
		60	720(75)	890	1560
		62	478(170)	170	1002
		64	491(75)	476	572
$\text{rms}_{\text{expt.} - \text{theor.}}$				205	662

tors were assumed to be zero. This is not strictly true, because of the vacancy in the $f_{7/2}$ shell, but the correction is less than the uncertainties.

The normalizations for proton spectroscopic factors, obtained by this process, are given in Table VI, with the rms variations between the values obtained for the four isotopes indicated. The momentum matching for the proton-transfer reactions is illustrated in Fig. 12 and we see that again, the $({}^3\text{He}, d)$ reaction is matched for $\ell = 1$ and not for higher values, while the (α, t) reaction is well matched for $\ell = 3$ and 4. The reactions were chosen accordingly to yield spectroscopic factors.

The $\ell = 3$ spectroscopic factors from the two reactions show a very similar pattern to that for neutrons, with reasonable consistency for strong transitions but discrepancies on the order of a factor of two for the weaker ones.

The vacancies obtained from proton transfer (under the assumption of a closed shell at $Z = 28$) are indicated in Fig. 13. It is evident that not all the $g_{9/2}$ strength was observed in this measurement, as may be expected

TABLE VI. Normalizations for proton transfer.

Reaction	ℓ -value	Normalization
$({}^3\text{He}, d)$	1	0.635 ± 0.042
$({}^3\text{He}, d)$	3	0.513 ± 0.069
(α, t)	3	0.450 ± 0.059

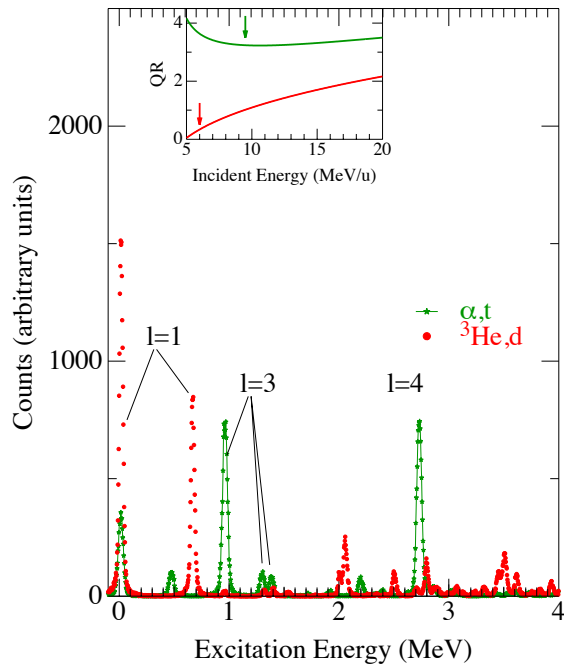


FIG. 12. (Color online) The inset illustrates momentum matching for the two proton-transfer reactions with the arrows indicating the bombarding energies used in the experiments, and Q is the momentum transfer and R the radius. Two spectra for the ${}^{62}\text{Ni}$ target, covering the same region of excitation energy, are shown.

because the first $9/2^+$ state occurs at 2.5-3 MeV excitation and the strength is likely to be fragmented more than that for states centered at lower excitation energies. The estimated uncertainties in cross sections for proton transfer are the same as for neutrons, the DWBA procedures in extracting spectroscopic factors have not been investigated quite as systematically as for neutron transfer, but the estimated uncertainties for spectroscopic factors are the same. These are listed in Appendix B, and the cross section data are available, as for neutron transfer [23]. The energy centroids for the proton excitation – including both isospin states and assuming the Coulomb-displacement energies of Ref. [28] – are shown in Fig. 14.

As to the closure of the $f_{7/2}$ shell for protons, the summed spectroscopic factors for proton addition going to $7/2^-$ states give a larger value than for neutrons. As is suggested by Fig. 10, this is consistent with the trend shown by neutrons, with the vacancies in the $f_{7/2}$ neu-

tron shell increasing as the target approaches ${}^{56}\text{Ni}$. The vacancies in the $f_{7/2}$ proton shell appear to be similar for the four Ni isotopes: 0.9, 0.9, 1.5 and 1.0 nucleons respectively. This then would imply that there must be substantial occupancy already in the $1p$ and/or $0f_{5/2}$ orbits. It is tempting to observe the difference in normalizations for $\ell = 1$ and 3 reactions: 0.635 and 0.513, respectively. If, as a limiting case, one were to assume that this occupancy is all in the $1p$ orbitals, and that the normalizations are the same for both values of ℓ , then the $\ell = 1$ spectroscopic factors would decrease by $\sim 19\%$ and the sums of these spectroscopic factors would decrease accordingly. Of course, this is not a unique solution. As was discussed above (e.g. in connection with Fig. 8) the relative normalizations for different j values depend on poorly defined assumptions about the bound-state parameters. For the neutron case each j value was normalized independently. For protons, it is probably more likely that both the $1p$ and the $0f_{5/2}$ orbitals have some partial occupancies; assuming that they share the missing occupancy equally would mean that all the corresponding spectroscopic factors are lower by $\sim 10\%$. There are some experiments [6] on proton-removal from the Ni isotopes that indicate summed spectroscopic strengths for $\ell = 1$ of about 0.5, but these were done at considerably higher energy and analyzed with different distorting and bound-state parameters, so that they are not directly comparable. No proton removal to $5/2^-$ states seems to have been identified, but there are a number of final states populated with $\ell = 3$ whose spins are not known. Thus the uncertainty for the proton measurements is greater than for neutrons; and while the numbers given here assume a perfect closed shell at $Z = 28$, it seems reasonable to expect that the values for spectroscopic factors could be 10-20% lower, with uncertainties that are also in that range.

III. COMPARISON WITH SHELL MODEL CALCULATIONS

Shell-model calculations were carried out for the energy levels in the final nuclei and to provide spectroscopic factors by using the shell-model code MSHELL [29]. Two interactions were used in the calculations that were fit to different data sets in this region. The GXPF1A [30] interaction is a slightly modified form of the GXPF1 [31] interaction based on nuclei in the mass range 47 and 66, and does not include the $0g_{9/2}$ in the model space. The second interaction JUN45 [32] was obtained by fitting data in the mass range between 63 and 96, with a somewhat different model space that included the $g_{9/2}$ state but not the $f_{7/2}$. The results are displayed in Figs. 15, 16 and 17. As was shown in Fig. 10 the GXPF1A interaction reproduces the pattern of behavior in the incompleteness of the $f_{7/2}$ shell. As indicated by the summed spectroscopic factors, the shell is violated worst just at $N, Z = 28$ and decreases the further the nucleus is away from 28. However, the absolute magnitudes from the

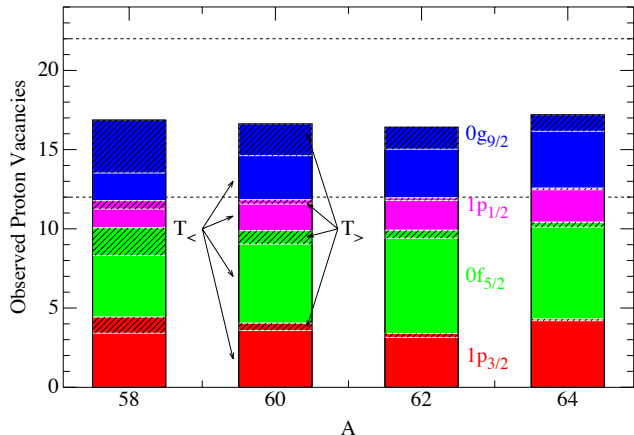


FIG. 13. (Color online) The vacancies in the proton orbits are shown orbit by orbit from the summed spectroscopic factors. The hatched area indicates the contribution from the $T_>$ component for each orbit, using the neutron-adding spectroscopic factors. A dashed line indicates the 12 protons that complete the $1p$ and $0f_{5/2}$ orbits; a second dashed line indicates the completeness of the $0g_{9/2}$ orbit at $Z = 50$. The observed strength for the $g_{9/2}$ orbit appears to be less than the full vacancy as discussed in the text. The $f_{7/2}$ strength is not included in the figure and the plot is subject to the ambiguities discussed in the text.

calculations are only about half the values obtained from the data.

The qualitative patterns of the states seem to be reproduced reasonably. However, the energy centroids pose some problems, as may be seen in Figs. 18 and 19. The centroid energies for $p_{3/2}$ and $f_{5/2}$ neutron transfer appear to be in reasonable agreement with the data, both for neutron addition and removal. However, the agreement with the $p_{1/2}$ energy centroids are not as good, particularly with the JUN45 interaction. For proton transfer the $p_{3/2}$ centroids are reproduced reasonably, but there appear to be problems with the proton centroids for both the $p_{1/2}$ and $f_{5/2}$ energies.

IV. SUMMARY

We have attempted to obtain a consistent set of spectroscopic factors for nucleon addition and removal on the four stable Ni isotopes.

With the normalization procedure used, the spectroscopic factors for neutron transfer are internally consistent at the level of a few percent, and do not depend on the fact that the closure of the $N = 28$ shell is not complete.

The same procedure could not be used for protons, where the completeness of the $Z = 28$ closed shell had

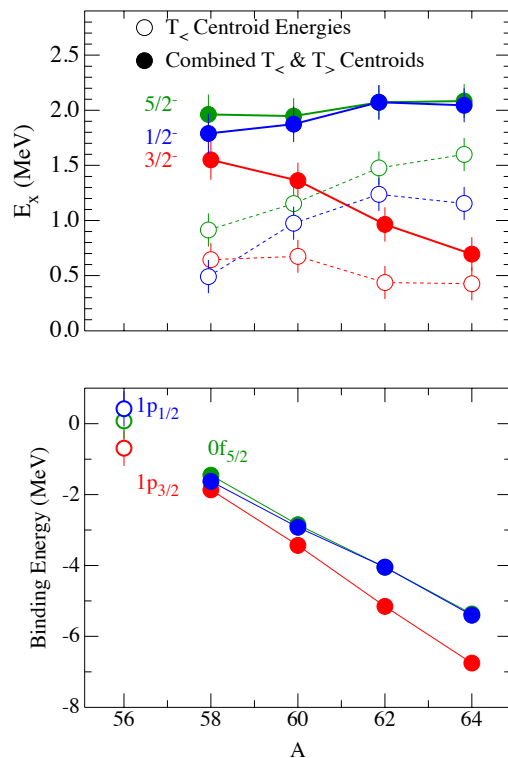


FIG. 14. (Color online) The energy centroids for proton-addition reactions probing the vacancies. The open symbols indicated the centroids for the $T_<$ states observed directly in proton transfer, while the full symbols show the isospin-averaged centroids, including the $T_>$ components computed from neutron transfer and assuming that all the strengths occurred as analog states at high excitation energy and from the known Coulomb Displacement energies. The lower part of the figure shows the same averaged centroids as a function of the binding energy of the last proton, and the open symbols are used for the single-particle energies that had been tentatively identified in earlier work, with some estimate of uncertainty.

to be assumed to start with. Since the data indicate that this assumption is not well satisfied in $Z = 28$ nuclei, this introduces inconsistencies and ambiguities in the normalization method on the order of 10%, and the uncertainties in proton spectroscopic factors are somewhat larger. As was stated in [1], even though spectroscopic factors may not strictly not strictly be true ‘observables’, the spectroscopic factors derived by our procedure yield occupancies and vacancies that are internally consistent for both neutrons and protons over the four Ni isotopes.

A comparison with shell-model calculations indicates reasonable, semi-quantitative agreement in the level structure and the values of the spectroscopic factors.

V. ACKNOWLEDGEMENTS

The authors wish to acknowledge John Greene for preparing the isotopic Ni targets and the operating staff

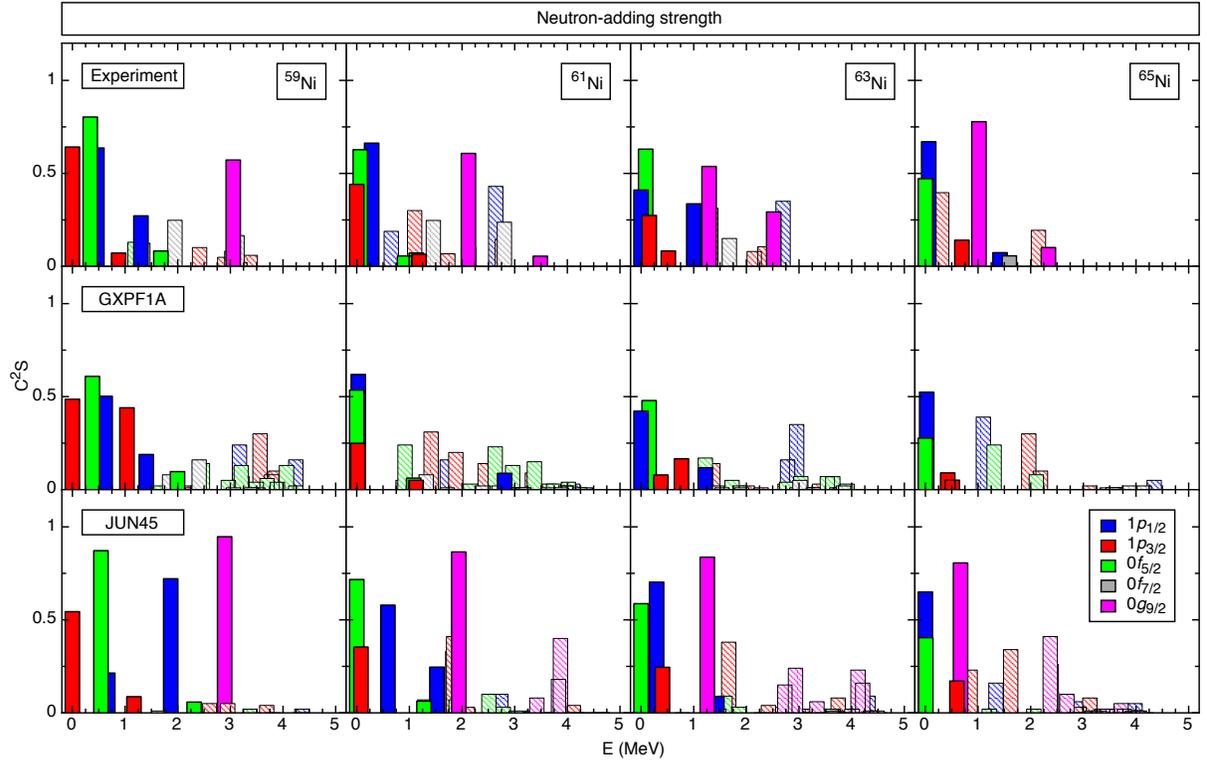


FIG. 15. (Color online) The experimental spectroscopic strengths, C^2S , for neutron addition are displayed on top. The color scheme is explained in the figure. The values of the strengths where $C^2S < 0.05$ have been multiplied by a factor of 10 and are displayed with hatching in the appropriate colors. The values calculated with two shell-model interaction are shown in the rows below and are also multiplied by this factor for the same transitions, using the experimental values as a criterion.

of the Yale tandem. This work was supported by the U.S. Department of Energy, Office of Nuclear Physics, under Contract No. DE-AC02-06CH11357 and Grant Nos. DE-FG02-91ER40609 and DE-FG02-04ER41320; NSF Grant No. PHY-08022648; and the U.K. Science and Technology Facilities Council.

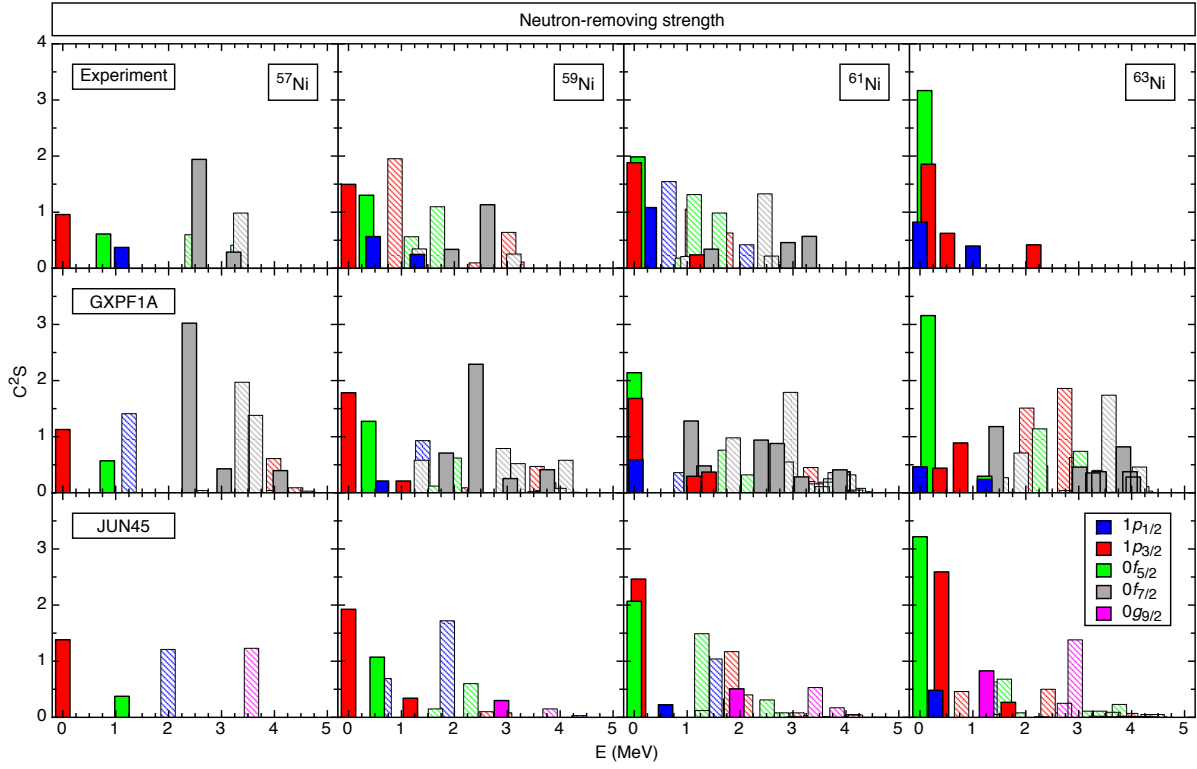


FIG. 16. (Color online) The spectroscopic strengths, C^2S , for neutron removal, with the arrangement and notation the same as in Fig. 15, except that here the strengths have been multiplied by a factor of 10 where $C^2S < 0.2$.

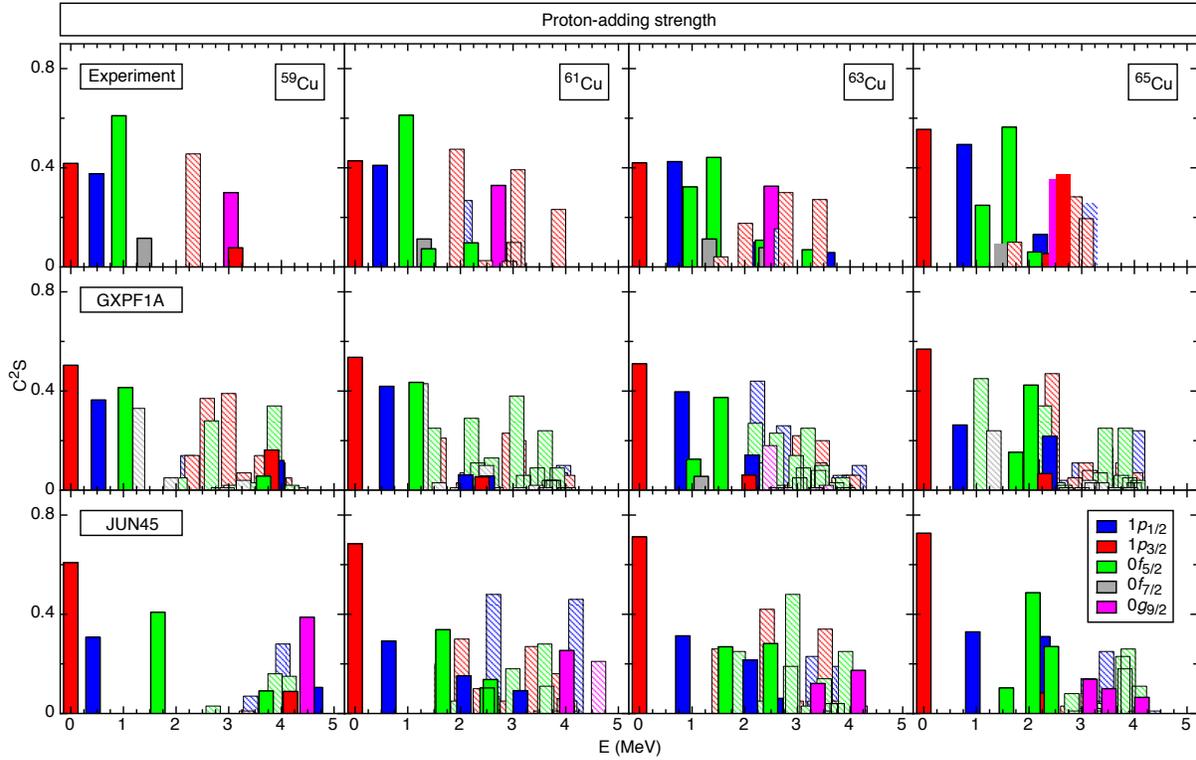


FIG. 17. (Color online) The spectroscopic strengths, C^2S , for proton adding, with the arrangement and notation the same as in Fig. 15, except that here the strengths have been multiplied by a factor of 10 where $C^2S < 0.05$.

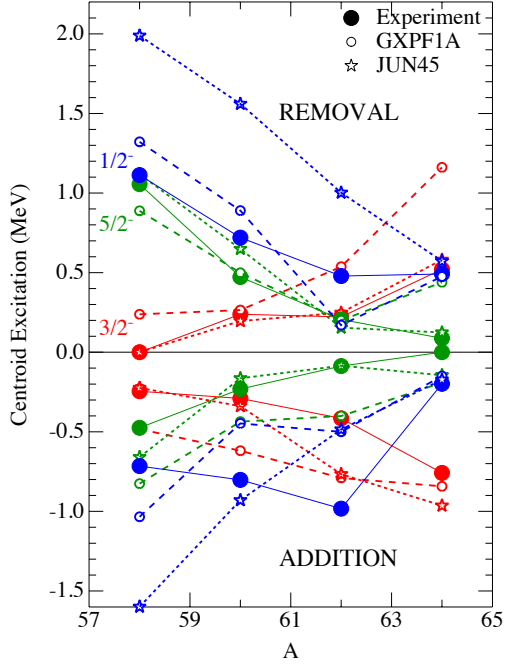


FIG. 18. (Color online) The energy centroids for neutron-addition reactions probing vacancies (shown as negative numbers) and neutron-removal reactions probing occupancies are plotted, along with the corresponding centroids from the two shell-model calculations.

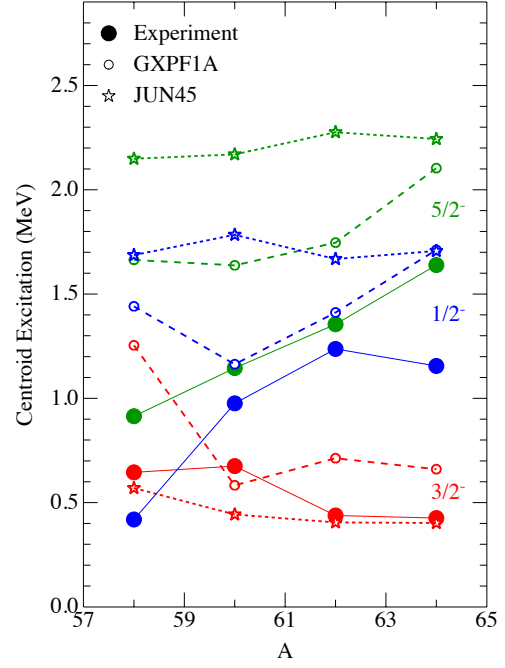


FIG. 19. (Color online) The energy centroids for proton vacancies from the proton-addition reactions are compared to the same quantities from the two shell-model calculations. The centroids are for the $T_{<}$ strengths.

Appendix A: Spectroscopic factors for neutron-adding and -removing reactions

The excitation energies and spins given below are taken from compilations [6] and are consistent with our measurements. The values of spectroscopic factors for $\ell = 1$ transitions are from the (d, p) and (p, d) reactions for the combination of potentials listed on the fourth line of Table IV. For $\ell = 3$ and 4 the spectroscopic factors are from the $(\alpha, {}^3\text{He})$ and $({}^3\text{He}, \alpha)$ reactions with the potentials from Refs. [25] and [26]. The reason for the latter choice was discussed in the text. Since the final nuclei have the same states from reactions on different targets, the tables here are grouped by *final* nucleus rather than the target.

A rough estimate of the uncertainties in spectroscopic factors has been given in the paper. For strong transitions that are greater than ~ 0.2 of the full single-particle value the uncertainty is estimated as about 10%, for transitions whose strength is between 0.03 and 0.2 $\sim 15\%$, and for transitions below 0.03 the uncertainty in S is 25% plus a constant value of about 0.005 in S for adding ($S/(2j+1)$ for removing). The relative values of spectroscopic factors for the stronger transitions are probably somewhat smaller – perhaps closer to the 4% uncertainties in cross sections.

TABLE VII. Neutron spectroscopic factors for states in ${}^{57}\text{Ni}$ from removing reactions.

E (keV)	j^π	C^2S
0	$3/2^-$	0.92
769	$5/2^-$	1.01
1113	$1/2^-$	0.18
2443	$5/2^-$	0.22
2577	$7/2^-$	4.95
3230	$7/2^-$	1.00
3311	$5/2^-, 7/2^-$	0.11
3364	$7/2^-$	0.32

TABLE VIII. Neutron spectroscopic factors for states in ${}^{59}\text{Ni}$ extracted from both the adding and removing reactions.

E (keV)	j^π	$(2j+1)C^2S$ [adding]	C^2S [removing]
0	$3/2^-$	2.46	1.49
339	$5/2^-$	4.42	1.85
465	$1/2^-$	1.22	0.28
878	$3/2^-$	0.28	0.20
1189	$5/2^-$	0.023	0.07
1301	$1/2^-$	0.52	0.12
1338	$7/2^-$	0.05	0.26
1680	$5/2^-$	0.78	0.24
1735	$3/2^-$	0.03	–
1948	$7/2^-$	0.09	0.65
2415	$3/2^-$	0.04	0.01
2627	$7/2^-$	–	2.63
2894	$3/2^-$	0.019	–
3026	$1/2^-, 3/2^-$	0.03	0.03
3054	$9/2^+$	3.75	–
3125	$7/2^-$	0.37	1.23
3182	$3/2^{(-)}$	0.03	0.011
3377	$1/2^-, 3/2^-$	0.023	–

TABLE IX. Neutron spectroscopic factors for states in ${}^{61}\text{Ni}$ extracted from both the adding and removing reactions.

E (keV)	j^π	$(2j+1)C^2S$ [adding]	C^2S [removing]
0	$3/2^-$	1.76	1.92
67	$5/2^-$	3.33	2.07
283	$1/2^-$	1.32	0.55
656	$1/2^-$	0.04	0.08
909	$5/2^-$	0.44	0.04
1015	$7/2^-$	–	0.009
1100	$3/2^-$	0.12	0.11
1132	$5/2^-$	0.40	0.18
1185	$3/2^-$	0.26	0.24
1455	$7/2^-$	0.16	0.54
1610	$5/2^-$	–	0.11
1729	$3/2^-$	0.027	0.06
2122	$9/2^+$	3.57	0.34
2124	$1/2^-$	0.21	0.04
2469	$7/2^-$	–	0.15
2593	$7/2^-$	–	0.03
2640	$1/2^-, 3/2^-$	0.09	0.011
2765	$3/2^-$	0.06	–
2801	$5/2^-, 7/2^-$	0.09	–
2905	$7/2^-$	0.08	0.80
3062	$1/2^+$	–	–
3308	$7/2^-$	–	1.11
3487	$9/2^+$	0.32	–

TABLE X. Neutron spectroscopic factors for states in ^{63}Ni extracted from both the adding and removing reactions.

E (keV)	j^π	$(2j+1)C^2S$ [adding]	C^2S [removing]
0	$1/2^-$	0.83	0.43
87	$5/2^-$	3.55	3.42
156	$3/2^-$	1.11	1.91
518	$3/2^-$	0.34	0.64
1001	$1/2^-$	0.68	0.41
1292	$(9/2)^+$	3.21	0.39
1324	$3/2^-$	0.13	–
1677	$(7/2^-)$	0.24	–
2149	$3/2^-$	0.03	0.43
2353	$(1/2^-, 3/2^-)$	0.04	–
2519	$(9/2)^+$	1.75	0.26
2697	$1/2^-$	0.07	–

TABLE XI. Neutron spectroscopic factors for states in ^{65}Ni from adding reactions.

E (keV)	j^π	$(2j+1)C^2S$
0	$5/2^-$	2.07
63	$1/2^-$	1.38
310	$3/2^-$	0.16
693	$3/2^-$	0.58
1017	$9/2^+$	4.27
1418	$1/2^-$	0.15
1594	$7/2^-$	0.14
2147	$3/2^-$	0.08
2336	$(9/2^+)$	0.56

Appendix B: Spectroscopic factors for proton-adding reactions

For proton transfer the potentials were taken from Ref. [25] for ^4He , Ref. [26] for ^3He , Ref. [12] for deuterons, and Ref. [33] for tritons, and here it is only for $\ell = 4$ that the (α, t) spectroscopic factors are cited, for $\ell = 1$ and 3 they are from the $(^3\text{He}, d)$ reaction. The relevant discussion of uncertainties in Appendix A for neutrons applies to the results for protons as well.

TABLE XII. Proton spectroscopic factors for states in ^{59}Cu .

E (keV)	j^π	$(2j+1)C^2S$
0	$3/2^-$	1.67
491	$1/2^-$	0.75
914	$5/2^-$	3.66
1399	$7/2^-$	0.93
2324	$3/2^{(-)}$	0.18
3043	$9/2^+$	–
3130	$3/2^-$	0.31

TABLE XIII. Proton spectroscopic factors for states in ^{61}Cu .

E (keV)	j^π	$(2j+1)C^2S$
0	$3/2^-$	1.71
475	$1/2^-$	0.82
970	$5/2^-$	3.67
1311	$7/2^-$	0.90
1394	$5/2^-$	0.44
1933	$3/2^-$	0.19
2089	$(1/2)^-$	0.054
2203	$5/2^-$	0.59
2358	$3/2^-$	0.065
2472	$3/2^-$	0.010
2721	$9/2^+$	3.29
2840	$1/2^-, 3/2^-$	0.38
2933	$3/2^-$	0.009
3019	$3/2^-$	0.040
3092	$3/2^-$	0.16
3863	$1/2^-, 3/2^-$	0.093

TABLE XIV. Proton spectroscopic factors for states in ^{63}Cu .

E (keV)	j^π	$(2j+1)C^2S$
0	$3/2^-$	1.68
670	$1/2^-$	0.85
962	$5/2^-$	1.94
1327	$7/2^-$	0.90
1412	$5/2^-$	2.65
1547	$3/2^-$	0.016
2013	$3/2^-$	0.070
2062	$(1/2)^-$	0.20
2337	$5/2^-$	0.65
2405	$7/2^-$	0.62
2505	$9/2^+$	3.26
2697	$1/2^-, 3/2^-$	0.062
2780	$1/2^-, 3/2^-$	0.12
3226	$(5/2^-)$	0.42
3426	$1/2^-, 3/2^-$	0.11
3575	$1/2^-, 3/2^-$	0.23

TABLE XV. Proton spectroscopic factors for states in ^{65}Cu .

E (keV)	j^π	$(2j+1)C^2S$
0	$3/2^-$	2.22
771	$1/2^-$	0.99
1116	$5/2^-$	1.49
1482	$7/2^-$	0.73
1623	$5/2^-$	3.38
1725	$3/2^-$	0.040
2107	$(5/2)^-$	0.36
2213	$(1/2)^-$	0.26
2329	$3/2^-$	0.21
2526	$9/2^+$	3.55
2650	$5/2^-, 7/2^-$	0.30
2874	$(3/2^-)$	0.11
3086	$(3/2^-)$	0.078
3157	$(1/2^-)$	0.051

- [1] J. P. Schiffer *et al.*, *Phys. Rev. Lett.* **108**, 022501 (2012).
- [2] M. H. Macfarlane and J. B. French, *Rev. Mod. Phys.* **32**, 567 (1960).
- [3] R. H. Fulmer and A. L. McCarthy, *Phys. Rev.* **131**, 2133 (1963).
- [4] S. Fortier and S. Galès, *Nucl. Phys.* **A321**, 137 (1979).
- [5] F. M. Edwards, J. J. Kraushaar, and B. W. Ridley, *Nucl. Phys.* **A199**, 463 (1973).
- [6] Evaluated Nuclear Structure Data File (ENSDF): <http://www.nndc.bnl.gov/ensdf/>.
- [7] P. Roussel *et al.*, *Nucl. Phys.* **A155**, 306 (1970).
- [8] R. M. Britton and D. L. Watson, *Nucl. Phys.* **A272**, 91 (1976).
- [9] J. P. Schiffer *et al.*, *Phys. Rev. Lett.* **100**, 112501 (2008).
- [10] A. Parikh, PhD Thesis, Yale University (2006).
- [11] M. H. Macfarlane and S. C. Pieper, Argonne National Laboratory, Report No. ANL-76-11, Rev. 1, 1978 (unpublished).
- [12] H. An and C. Cai, *Phys. Rev.* **73**, 054605 (2006).
- [13] F. D. Becchetti and G. W. Greenlees, *Phys. Rev.* **182**, 1190 (1969).
- [14] A. J. Koning and J. P. Delaroche, *Nucl. Phys.* **A713**, 231 (2003).
- [15] C. J. Batty and G. W. Greenlees, *Nucl. Phys.* **A133**, 673 (1969).
- [16] R. H. Bassel *et al.*, *Phys. Rev.* **136**, B960 (1964).
- [17] W. W. Daehnick, J. D. Childs, and Z. Vrcelj, *Phys. Rev. C* **21**, 2253 (1980).
- [18] C. M. Perey and F. G. Perey, *Phys. Rev.* **132**, 755 (1963).
- [19] F. G. Perey, *Phys. Rev.* **131**, 745 (1963).
- [20] G. W. Greenless, G. J. Pyle, and Y. C. Tang, *Phys. Rev. Lett.* **17**, 33 (1966).
- [21] L. Lapikás, *Nucl. Phys.* **A553**, 297 (1993).
- [22] V. R. Pandharipande, I. Sick, and P. K. A. deWitt Huberts, *Rev. Mod. Phys.* **69**, 981 (1997).
- [23] Experimental Unevaluated Nuclear Data List (XUNDL): <http://www.nndc.bnl.gov/xundl/>.
- [24] B. P. Kay *et al.*, *Phys. Rev. C* **79**, 021301(R) (2009).
- [25] G. Bassani and J. Picard, *Nucl. Phys.* **A131**, 653 (1969).
- [26] C. M. Perey and F. G. Perey, *At. Data Nucl. Data Tables* **17**, 1 (1976).
- [27] J. P. Schiffer, *Isospin in Nuclear Physics*, p. 665 D. H. Wilkinson, editor, North-Holland Publishing Co. 1969.
- [28] J. A. Nolen and J. P. Schiffer, *Ann. Rev. Nucl. Sci.* **19** 471 (1969).
- [29] T. Mizusaki, RIKEN Accel. Prog. Rep. **33**, 14 (2000).
- [30] M. Honma, T. Otsuka, B. A. Brown, and T.M. Mizusaki, *Eur. Phys. J. A* **25**, Supplement 1, 499 (2005).
- [31] M. Honma, T. Otsuka, B. A. Brown, and T. M. Mizusaki, *Phys. Rev. C* **69**, 034335 (2004).
- [32] M. Honma, T. Otsuka, T. Mizusaki, and M. Hjorth-Jensen, *Phys. Rev. C* **80**, 064323 (2009).
- [33] E. R. Flynn *et al.*, *Phys. Rev. C* **28**, 575 (1983).